ANL-HEP-PR-03-057
EFI-03-39

Beautiful Mirrors, Unification of Couplings and Collider Phenomenology

D.E. Morrissey[a,b], and **C.E.M. Wagner**[a,b]

[a] *HEP Division, Argonne National Laboratory, 9700 Cass Ave., Argonne, IL 60439, USA*
[b] *Enrico Fermi Institute, Univ. of Chicago, 5640 Ellis Ave., Chicago, IL 60637, USA*

August 4, 2003

Abstract

The Standard Model provides an excellent description of the observables measured at high energy lepton and hadron colliders. However, measurements of the forward-backward asymmetry of the bottom quark at LEP suggest that the effective coupling of the right-handed bottom quark to the neutral weak gauge boson is significantly different from the value predicted by the Standard Model. Such a large discrepancy may be the result of a mixing of the bottom quark with heavy mirror fermions with masses of the order of the weak scale. To be consistent with the precision electroweak data, the minimal extension of the Standard Model requires the presence of vector-like pairs of $SU(2)$ doublet and singlet quarks. In this article, we show that such an extension of the Standard Model is consistent with the unification of gauge couplings and leads to a very rich phenomenology at the Tevatron, the B-factories and the LHC. In particular, if the Higgs boson mass lies in the range 120 GeV $\lesssim m_h \lesssim$ 180 GeV, we show that Run II of the Tevatron collider with 4–8 fb^{-1} of integrated luminosity will have the potential to discover the heavy quarks, while observing a 3-σ evidence of the Higgs boson in most of the parameter space.

1 Introduction

In the absence of direct evidence for physics beyond the Standard Model (SM), precision electroweak tests are the best way to get information about the scale and nature of a possible breakdown of the SM description. While the SM has held firm in the face of a great number of precision electroweak tests, the model has not emerged completely unscathed. Fits of the SM to electroweak data show about a 2.5-σ deviation in the b-quark forward-backward asymmetry (A_{FB}^b) [1], and this situation has not improved much in the last five years. This discrepancy is important for two reasons. On one hand, it seems to indicate a significant deviation of the coupling of the right-handed bottom quark to the Z-gauge boson (see, for example, Ref. [2]). On the other, this measurement plays an important role in the present fits to the SM Higgs mass; the removal of the heavy quark data from the electroweak fits would push the central values of the Higgs mass to lower values, further inside the region excluded by the LEP2 searches [3].

There are two ways of solving this apparent discrepancy, and both of them seem to indicate the presence of new physics. In Ref. [4] it was proposed to exclude the heavy quark data while introducing new physics that raises the central value of the Higgs boson mass, and improves the fit to the other observables. Such a task requires new physics that gives a negative contribution to the S parameter, positive contributions to the U parameter and a moderate contribution to the T parameter. At least two examples of this kind of physics have been presented in the literature [4], [5]; the first within low energy supersymmetry and the second within a warped extra-dimension scenario.

An alternative to this procedure is to take seriously the heavy quark data while introducing new physics that modifies in a significant way the right-handed bottom quark coupling to the Z. The Beautiful Mirror model of Ref. [6] accomplishes this by allowing the b-quark to mix strongly with a set of exotic vector-like quarks. This model turns out to have several other interesting features which we investigate in this paper. To be specific, we consider the unification of gauge couplings, additional patterns of flavour mixing, the Higgs phenomenology, and searches for the heavy vector quarks.

The model consists of the SM plus additional vector-like "mirror" quarks. These are a pair of $SU(2)$ doublets, $\Psi_{L,R} = \binom{\chi'_{L,R}}{\omega'_{L,R}}$, and a pair of $SU(2)$ singlets, $\xi'_{L,R}$. Here and in what follows we use primed fields to denote gauge eigenstates, while mass eigenstates are written as unprimed fields. The gauge group quantum numbers are the same as those of the analogous SM particles: $(3, 2, 1/6)$ for the doublets, and $(3, 1, -1/3)$ for the singlets. Since the quarks are

added in vector-like pairs, these can have gauge-invariant Dirac masses, and the model is free of anomalies. This is a minimal set of mirror quarks needed to improve the fit to electroweak data.

The Yukawa and mass couplings of the mirror quarks are taken to be

$$\begin{aligned}\mathscr{L} \supset & -(y_b\bar{Q}'_L + y_2\bar{\Psi}'_L)b'_R\Phi - (y_t\bar{Q}'_L + y_4\bar{\Psi}'_L)t'_R\tilde{\Phi} - M_1\bar{\Psi}'_L\Psi'_R \\ & - (y_3\bar{Q}'_L + y_5\bar{\Psi}'_L)\xi'_R\Phi - M_2\bar{\xi}'_L\xi'_R + (h.c.)\end{aligned} \tag{1}$$

where $Q'_L = \binom{t'_L}{b'_L}$ is the usual third generation SM quark doublet, and $\Phi = \binom{\phi^+}{\phi^0}$ is the Higgs doublet. This is the most general set of renormalizable couplings provided the mirror quarks couple only to each other and to the third SM generation.[1] As pointed out in [6], the Yukawa couplings y_b, y_3 and y_4 are constrained to be much smaller than y_2. Adjusting the ratio $(\frac{v}{\sqrt{2}}y_2)/M_1 \simeq 0.7$, where $v = 246.22$ GeV is the Higgs VEV, gives the best fit to precision electroweak data while reducing the discrepancy in A^b_{FB} to about one standard deviation, and keeping the left-right b-quark asymmetry measured at SLC within one standard deviation of the measured value. This forces y_2 to be $\mathcal{O}(1)$ since $M_1 \gtrsim 200$ GeV is needed to explain why mirror quarks have not yet been observed. On the other hand, there are no strong constraints on y_5. As in [6], we will neglect it for simplicity.

This paper consists of seven sections. In Section 2 we examine the running of the gauge couplings and their unification at a high scale. In section 3 we discuss the issue of flavour mixing as well as the quark couplings to the neutral and charged weak gauge bosons, and the Higgs. Section 4 consists of an investigation of the Higgs phenomenology in the model. In Section 5 we review the current limits on exotic quarks and investigate the possibility of finding mirror quarks at the Tevatron. In Section 6 we examine how the new types of flavour mixing possible with mirror quarks can affect CP violation in $B \to \phi K_s$ decays. Finally, Section 7 is reserved for our conclusions.

2 Unification of Gauge Couplings

The idea that the low energy gauge forces proceed from a single grand unified description is a very attractive one, and is supported by the apparent convergence of the weak, hypercharge and strong couplings at short distances. The interest in low energy supersymmetry, for instance, has been greatly enhanced by the discovery that the value of the strong coupling, $\alpha_s(M_Z)$,

[1] Note that couplings like $\bar{Q}'_L\Psi'_R$ and $\bar{\xi}'_Lb'_R$ can be rotated away.

can be deduced if one assumes that the gauge couplings unify at a high scale. This prediction depends on model-dependent threshold corrections at the GUT scale, but to within the natural uncertainty in these corrections [18] the predicted value of $\alpha_s(M_Z)$ is perfectly consistent with the values measured at low energies. In the Standard Model, instead, the assumption of gauge coupling unification leads to a prediction for $\alpha_s(M_Z)$ that differs from the measured value by an amount that is well beyond the natural uncertainties induced by threshold corrections.

In [6] it was noted that, to one-loop order, adding mirror quarks of the type considered here to the SM greatly improves the prediction of $\alpha_s(M_Z)$ based on the assumption of gauge coupling unification. We extend this analysis by including the two-loop contributions to the gauge coupling beta functions and the low-scale threshold corrections. Since, for the consistency of this study, the Higgs sector must remain weakly-coupled while the Higgs potential should remain stable up to scales of the order of the unification scale, M_G, we also investigate the related issues of stability and perturbative consistency of the Higgs sector.

In extrapolating the low energy description of the theory to short distances, it is important to remark that the Beautiful Mirror model [6] does not provide a solution to the hierarchy problem. Therefore, a main assumption behind this extrapolation is that the physics that leads to an explanation of the hierarchy problem does not affect the connection of the low energy couplings to the fundamental ones. An example of such a theory construction is provided by warped extra dimensions [7], and has been investigated by several authors [8]–[10]. In order to preserve the good agreement with the precision electroweak data, the Kaluza-Klein modes must be heavier than a few TeV in this case [11], and therefore the low energy physics analyzed in the subsequent sections will not be affected. On the other hand, extra dimensions could modify the proton decay rate in a significant way by introducing new baryon number violating operators, and, in the case of warped extra dimensions with a Higgs field located in the infrared brane, would make the issue of the running of the Higgs quartic coupling an irrelevant one. For the rest of this section, we shall proceed with a pure four dimensional analysis of the evolution of couplings and of the proton decay rate.

2.1 Renormalization Group Equations

Using the results of [12, 13], the two-loop ($\overline{MS}$ scheme) gauge coupling beta functions are

$$\beta_l = \frac{dg_l}{dt} = -\frac{1}{(4\pi)^2} b_l g_l^3 - \frac{1}{(4\pi)^4} \sum_{k=1}^{3} b_{kl} g_k^2 g_l^2 - \frac{1}{(4\pi)^4} g_l^3 Y_4^l(F) \tag{2}$$

where $t = \ln\left(\frac{\mu}{M_Z}\right)$ is the energy scale, and $l = 1, 2, 3$ refers to the U(1), SU(2), and SU(3) gauge groups respectively. The first term is the one-loop contribution, while the other terms come from two-loop corrections.

The coefficients b_l and b_{kl} are given by

$$b_1 = -\tfrac{9}{2}, \quad b_2 = \tfrac{7}{6}, \quad b_3 = 5, \tag{3}$$

and

$$b_{kl} = -\begin{pmatrix} \frac{291}{25} & 1 & \frac{13}{10} \\ 3 & \frac{91}{3} & \frac{15}{2} \\ \frac{52}{5} & 20 & 12 \end{pmatrix}. \tag{4}$$

In the SM, the corresponding one-loop beta function coefficients are $b_1^{SM} = -41/10$, $b_2^{SM} = 19/6$ and $b_3^{SM} = 7$. The variation of these coefficients are hence $\Delta b_1 = 2/5$ and $\Delta b_2 = \Delta b_3 = 2$. Since b_2 and b_3 are shifted by an equal amount, they tend to unify at the same scale as in the SM, about a few times 10^{16} GeV. Interestingly enough, the shift in b_1 is much smaller than that of b_2 and b_3, leading to, as we shall see, a successful unification of the three couplings.

The coefficients $Y_4^l(F)$ involve the Yukawa couplings. Neglecting the small Yukawa couplings y_b, y_3, y_4, and y_5, they are

$$Y_4^l(F) = C_{lt} {y_t}^2 + C_{l2} {y_2}^2 \tag{5}$$

where

$$C_{lf} = \begin{pmatrix} \frac{17}{10} & \frac{1}{2} \\ \frac{3}{2} & \frac{3}{2} \\ 2 & 2 \end{pmatrix} \tag{6}$$

and f = t,2.

The Yukawa couplings evolve according to

$$(4\pi)^2 \frac{dy_f}{dt} = \beta_f y_f \tag{7}$$

where $f = t, 2$. The one-loop and leading two-loop contributions to β_f were calculated following [14]. Of the two-loop terms, we include only those involving g_3 or the Higgs self coupling λ; the g_3 terms are enhanced by large colour factors while the λ terms can become important when investigating the stability of this coupling. The one-loop contributions are

$$\begin{aligned} (4\pi)^2 \beta_t^{(1)} &= \frac{9}{2} y_t^2 + 3 y_2^2 - \left(\frac{17}{20} g_1^2 + \frac{9}{4} g_2^2 + 8 g_3^2 \right), \\ (4\pi)^2 \beta_2^{(1)} &= \frac{9}{2} y_2^2 + 3 y_t^2 - \left(\frac{1}{4} g_1^2 + \frac{9}{4} g_2^2 + 8 g_3^2 \right). \end{aligned} \tag{8}$$

The two-loop contributions that we have included are

$$\begin{aligned}(4\pi)^4\beta_t^{(2)} &= \frac{3}{2}\lambda^2 - 6y_t^2\lambda + g_3^2(46y_t^2 + 20y_2^2) - \frac{284}{3}g_3^4, \\ (4\pi)^4\beta_2^{(2)} &= \frac{3}{2}\lambda^2 - 6y_2^2\lambda + g_3^2(20y_t^2 + 46y_2^2) - \frac{284}{3}g_3^4. \end{aligned} \tag{9}$$

The total beta-function is the sum of these pieces: $\beta_f = \beta_f^{(1)} + \beta_f^{(2)}$. Aside from the modifications due to the mirror quarks, these are in agreement with the results of [12].

The Higgs self-coupling λ is taken to be

$$\mathscr{L} \supset \mu^2\Phi^\dagger\Phi - \frac{1}{2}\lambda(\Phi^\dagger\Phi)^2. \tag{10}$$

With this definition, the tree-level Higgs mass is $m_h = \sqrt{\lambda}v$, where $v = 246.22$ GeV $= \sqrt{2}\langle\phi^0\rangle$. λ evolves according to $\frac{d\lambda}{dt} = \beta_\lambda$. We have calculated the one-loop and leading two-loop contributions to β_λ using the results of [15, 16]. As for the Yukawas, only the largest two-loop terms involving g_3 or λ were included. For the one-loop part, we obtain

$$\begin{aligned}(4\pi)^2\beta_\lambda^{(1)} &= 12\lambda^2 - \left(\frac{9}{5}g_1^2 + 9g_2^2\right)\lambda + \frac{9}{4}\left(\frac{3}{25}g_1^4 + \frac{2}{5}g_1^2g_2^2 + g_2^4\right) \\ &\quad + 12\lambda\left(y_t^2 + y_2^2\right) - 12\left(y_t^4 + y_2^4\right). \end{aligned} \tag{11}$$

The two loop part is given by

$$\begin{aligned}(4\pi)^4\beta_\lambda^{(2)} &= -78\lambda^3 - 72(y_t^2 + y_2^2)\lambda^2 - 3(y_t^4 + y_2^4)\lambda + 60(y_t^6 + y_2^6) \\ &\quad + 18(\frac{3}{5}g_1^2 + 3g_2^2)\lambda^2 + 80g_3^2(y_t^2 + y_2^2)\lambda - 64g_3^2(y_t^4 + y_2^4). \end{aligned} \tag{12}$$

Again, the total beta-function is the sum of the one- and two-loop parts.

2.2 Input Parameters and Threshold Corrections

We have investigated the running of these couplings numerically. The initial values $\overline{MS}$ scheme values were taken from [17]:

$$\begin{array}{rclrcl} \alpha^{-1}(M_Z) &=& 127.922 \pm 0.027 & \sin^2\theta_w(M_Z) &=& 0.23113 \pm 0.00015 \\ M_Z &=& 91.1876 \pm 0.0021 & v &=& 246.22 \text{ GeV} \\ \bar{m}_t(m_t) &=& 165 \pm 5 \text{ GeV}. & & & \end{array} \tag{13}$$

These parameters correspond to the effective $SU(3)_c \times U(1)_{em}$ theory with five quarks obtained by integrating out the heavy gauge bosons and quarks in the full $SU(3)_c \times SU(2) \times U(1)_Y$ theory

at scale M_Z. Threshold corrections to the gauge couplings arise in the process of matching the theories. We define

$$\begin{aligned} \tilde{\alpha}_1^{-1} &= \frac{3}{5}(1-\sin^2\theta_w)\alpha^{-1}, \\ \tilde{\alpha}_2^{-1} &= \sin^2\theta_w\alpha^{-1}, \\ \tilde{\alpha}_3^{-1} &= \alpha_s^{-1}. \end{aligned} \tag{14}$$

Then the gauge couplings at M_Z are given by

$$\alpha_l^{-1} = \tilde{\alpha}_l^{-1} + \rho_l, \tag{15}$$

where the ρ_l terms represent threshold corrections. To one-loop order, these are[18]

$$\begin{aligned} \rho_3 &= \frac{1}{3\pi}\sum_\zeta \ln(\frac{m_\zeta}{M_z}), \\ \rho_2 &= \sin^2\theta_w\left[\frac{1}{6\pi}(1-21\ln(\frac{M_W}{M_Z})) + \frac{2}{\pi}\sum_\zeta Q_\zeta^2\ln(\frac{m_\zeta}{M_Z})\right], \\ \rho_1 &= \frac{3}{5}\left(\frac{1-\sin^2\theta_w}{\sin^2\theta_w}\right)\rho_2, \end{aligned} \tag{16}$$

where the sums run over $\zeta = t, \chi, \omega, \xi$. As shown in [6], the tree-level masses of the mirror quarks are given by

$$\begin{aligned} m_\chi &= M_1, \qquad m_\omega = (M_1^2 + Y_2^2)^{1/2}, \\ m_\xi &= M_2, \end{aligned} \tag{17}$$

where $Y_2 = \frac{v}{\sqrt{2}}y_2$. These parameters are not completely independent. As explained above, $Y_2 \simeq 0.7\ M_1$ gives the best fit to electroweak data, while $M_2, M_1 \gtrsim 200$ GeV are needed to explain why these exotics have not yet been observed at the Tevatron[35] (see section 5).

2.3 Numerical Evolution

The unification of gauge couplings was investigated by fixing $\sin^2\theta_w(M_Z)$ and $\alpha_{em}(M_Z)$ according to their measured values, and varying $\alpha_s(M_Z)$ until the gauge couplings unified to within 1%. GUT-scale threshold corrections were not considered. Figure 1 shows the range of $\alpha_s(M_Z)$ obtained in this way for 250 GeV $\leq M_2 \leq$ 1000 GeV and all values of $\lambda(M_Z)$ and $y_2(M_Z)$ consistent with unification. (See the following section.) The range is plotted against the unification scale. In general, the unification is quite insensitive to the input values of M_2, λ, and

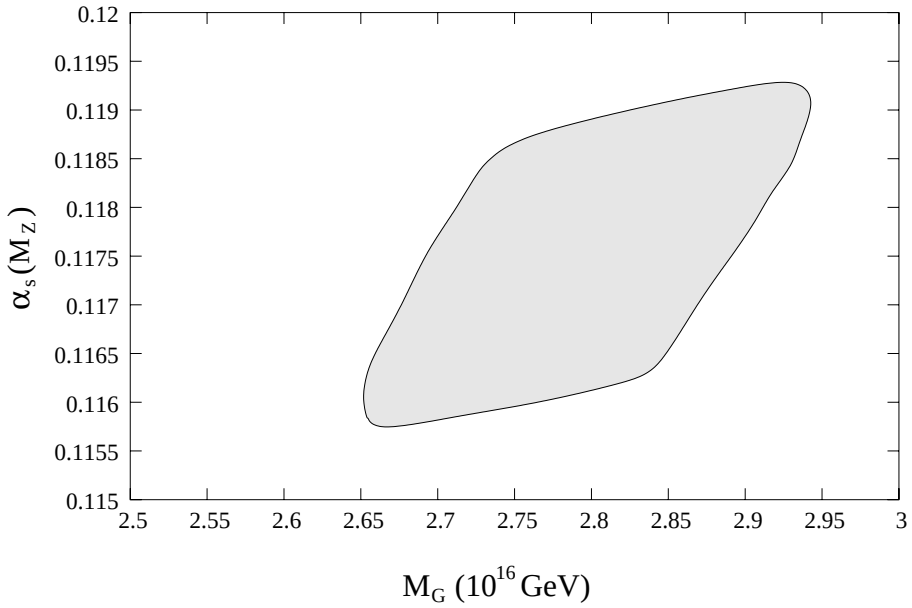

Figure 1: Range of α_s consistent with a 1% unification of the gauge couplings plotted against the unification scale M_G.

y_2. The scale of unification is quite high, $M_G = (2.80 \pm 0.15) \times 10^{16}$ GeV, depending on the input values, at which point the unified gauge coupling constant has value $\alpha_G^{-1} = 35.11 \pm 0.05$.

The predicted range of the strong gauge coupling is in excellent agreement with the values measured experimentally. This agreement is quite intriguing since the particular completion of the Standard Model considered in this work is motivated by data and not by any model building consideration. We shall not attempt to construct a grand unified model leading to the appearance of the mirror quarks considered here in the low energy spectrum. Instead, we will concentrate on additional issues regarding the renormalization group evolution of the dimensionless couplings of the theory, as well as on exploring general features of the low energy phenomenology of this particular extension of the Standard Model.

2.4 Stability and Non-Triviality of the Higgs

If the extrapolation of the model up to high scales is to be self-consistent, it should remain stable and weakly-coupled up to the unification scale. The only source of trouble in this regard is the Higgs self-coupling λ. Stability of the Higgs sector requires $\lambda(Q) > 0$, for all $Q < M_G$ while

perturbative consistency means that λ must not be too large. For concreteness we demand [2] that $0 < \lambda < 2$ up to 10^{17} GeV. This is sufficient to guarantee that the effective potential is similarly well behaved [19]. The evolution of λ is largely determined by the initial values of y_2 and λ. Only for a small subset of initial values does λ remain well-behaved (i.e. $0 < \lambda < 2$) up to M_G. This subset is shown in Figure 2, where we have written λ in terms of the (tree-level) Higgs mass, and Y_2 in terms of m_χ assuming $Y_2 = 0.7M_1$.

We compare the allowed region with the region favoured by precision electroweak data found in [6]. There is a small overlap between the allowed band found here and the 1-σ allowed region of [6] corresponding to $m_h \sim 170$ GeV and $m_\chi \sim 200$ GeV ($m_\omega \sim 250$ GeV).

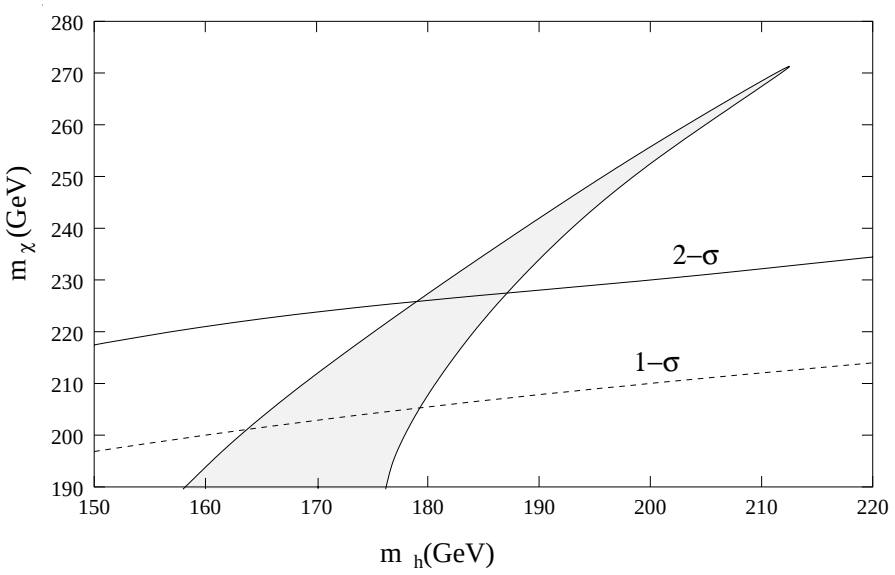

Figure 2: Region in the m_h-m_χ plane that is consistent with unification (shaded region) and precision electroweak data (below the dashed and solid lines).

2.5 Proton Decay

Grand unified models induce baryon number violating operators that lead to a proton decay rate that may be observable in the next generation of proton decay experiments. The present bounds on the proton lifetime [20] already put relevant bounds on grand unified scenarios. In four dimensional supersymmetric grand unified models, for instance, dimension five operators

[2]This upper limit on λ is somewhat arbitrary but fairly unimportant in the present case since λ grows very quickly when it becomes larger than unity.

may easily induce a proton lifetime shorter than the present experimental bound [21]. This situation may be avoided by a suitable choice of the low energy spectrum [22]. Heavy first and second generation sfermions and light gauginos are preferred from these considerations.

In the model under study there are no dimension-five operators, so the dominant decay mode is expected to be $p \to \pi^0 e^+$. The high unification scale obtained above means that the proton will be long-lived regardless of the details of the unification mechanism. If proton decay proceeds via $SU(5)$ gauge bosons, the decay rate is given by [23]

$$\Gamma(p \to \pi^0 e^+) = \frac{\pi m_p \alpha_G^2}{8 f_\pi^2 M_G^4}(1+D+F)^2 \alpha_N^2 \left[A_R^2 + (1+|V_{ud}|^2)^2 A_L^2\right] \tag{18}$$

where $f_\pi = 0.131$ GeV is the pion decay constant, $D = 0.81$ and $F = 0.44$ are chiral Lagrangian factors, α_N is a coefficient related to the $\pi^0 p$ operator matrix element, and A_L and A_R are correction factors due to the running of the couplings. A recent lattice-QCD calculation gives [24] $|\alpha_N| = 0.015(1)$ GeV^3, where the uncertainty is purely statistical. The systematic uncertainty is probably much larger; we take it to be $\sim 50\%$ [22]. The correction factors $A^{L,R}$ split into long and short distance pieces: $A_{L,R} = A_l \prod_{i=1}^3 A_i^{L,R}$, where A_l comes from the renormalization group evolution below M_Z and $A_i^{L,R}$ from that above. Here, $A_l \simeq 1.3$ is identical to the SM value, while the short distance pieces, to one-loop order, are [25]

$$\begin{aligned}
A_3^L &= \left[\frac{\alpha_3(M_Z)}{\alpha_G}\right]^{6/(33-4n_g-6)} \simeq 3.15 = A_3^R, \\
A_2^L &= \left[\frac{\alpha_2(M_Z)}{\alpha_G}\right]^{27/(86-16n_g-24)} \simeq 1.39 = A_2^R, \\
A_1^L &= \left[\frac{\alpha_1(M_Z)}{\alpha_G}\right]^{-69/(6+80n_g+24)} \simeq 1.14, \\
A_1^R &= \left[\frac{\alpha_1(M_Z)}{\alpha_G}\right]^{-33/(6+80n_g+24)} \simeq 1.07.
\end{aligned} \tag{19}$$

Using $M_G = 2.8 \times 10^{16}$ GeV, and $\alpha_G^{-1} = 35.1$, we find

$$\tau(p \to \pi^0 e^+) = 3 \times 10^{36\pm1} \text{yrs}, \tag{20}$$

well in excess of the Super-Kamiokande bound of $\tau(p \to \pi^0 e^+) = 5.3 \times 10^{33}$ yrs [20].

3 Flavour Mixing

Extending the matter content of the SM also introduces new sources of flavour mixing. With mirror quarks, this pattern can be quite complicated, involving right-handed couplings to the

W, and tree-level flavour-changing couplings to the Z and the Higgs. We consider first the generic case, taking the most general set of Yukawa and mass terms possible. Next, we simplify our results making use of the fact that, in the model under study, the mirror quarks couple only to the third generation quarks and calculate explicitly the couplings of the heavy quarks to the weak gauge bosons and the Higgs. In subsequent sections we shall use these results to investigate the Higgs phenomenology, the collider searches for mirror quarks, and CP violation in $B \to \phi K_s$ decays.

Let λ_u and λ_d be the flavour-space mass matrices describing the flavour mixing between gauge eigenstates. These matrices will be 4×4 and 5×5 respectively, and will have contributions from Yukawa couplings and Dirac mass terms. Both matrices can be diagonalized by bi-unitary transformations:

$$\lambda_u = U_u D_u W_u^\dagger, \quad \lambda_d = U_d D_d W_d^\dagger, \tag{21}$$

where the U's and W's are unitary, and D_u and D_d are the diagonalized mass matrices. The corresponding (unprimed) mass eigenstates are then related to the (primed) gauge eigenstates by the unitary transformations

$$\begin{array}{ll} {u'}_L^A = U_u^{AB} u_L^B, & {u'}_R^A = W_u^{AB} u_R^B, \\ {d'}_L^P = U_d^{PQ} d_L^Q, & {d'}_R^P = W_d^{PQ} d_R^Q. \end{array} \tag{22}$$

Here, the indices $A, B = 1, \ldots 4$ correspond to $\{u, c, t, \chi\}$, while $P, Q = 1, \ldots 5$ refer to $\{d, s, b, \omega, \xi\}$ respectively.

In terms of the physical (mass eigenstate) fields, the charged currents become

$$\begin{aligned} \sqrt{2} J^\mu_{W^+} &= \bar{u}_L^B \gamma^\mu V_L^{BQ} d_L^Q + \bar{u}_R^B \gamma^\mu V_R^{BQ} d_R^Q, \\ J^\mu_{W^-} &= {J^\mu_{W^+}}^\dagger, \end{aligned} \tag{23}$$

where the 4×5 flavour-mixing matrices are given by

$$\begin{aligned} V_L^{BQ} &= \sum_{i=1}^{4} U_u^{iB*} U_d^{iQ}, \\ V_R^{BQ} &= W_u^{B4*} W_d^{4Q}. \end{aligned} \tag{24}$$

The matrix V_L is analogous to the CKM matrix V_{CKM} of the SM. It is nearly unitary in the sense that $V_L {V_L}^\dagger = \mathbb{I}_{4\times4}$ and $V_L^\dagger V_L = \mathbb{I}_{5\times5} - V_d$, where the matrix V_d is defined below. The matrix V_R describes right-handed couplings, and has no analogue in the SM.

Similarly, the hadronic neutral current is

$$\begin{aligned}\cos\theta_w J_Z^\mu &= \bar{u}_L^A\gamma^\mu(\frac{1}{2}-\frac{2}{3}\sin^2\theta_w)u_L^A+\bar{u}_R^A\gamma^\mu(-\frac{2}{3}\sin^2\theta_w)u_R^A \\ &+\bar{d}_L^P\gamma^\mu(-\frac{1}{2}+\frac{1}{3}\sin^2\theta_w)d_L^P+\bar{d}_R^P\gamma^\mu(\frac{1}{3}\sin^2\theta_w)d_R^A \\ &+\frac{1}{2}\left(\bar{u}_R^A\gamma^\mu V_u^{AB}u_R^B-\bar{d}_R^P\gamma^\mu\tilde{V}_d^{PQ}d_R^Q+\bar{d}_L^P\gamma^\mu V_d^{PQ}d_L^Q\right) \qquad (25)\end{aligned}$$

where the matrices $V_u, V_d, \tilde{V}_d$ are given by

$$\begin{aligned}V_u^{AB} &= W_u^{4A*}W_u^{4B}, \qquad (26)\\ V_d^{PQ} &= U_d^{5P*}U_d^{5Q},\\ \tilde{V}_d^{PQ} &= W_d^{4P*}W_d^{4Q}.\end{aligned}$$

The off-diagonal elements of these matrices describe FCNCs. Each is Hermitian and satisfies $V^2 = V$.

3.1 Heavy Quark Neutral and Charged Currents

The expressions above can be simplified considerably by using the fact that, in the model under study, the (gauge eigenstate) mirror quarks couple only to the quarks of the third generation (see Eq. (1)). The mixing between the mirror quarks and the first and second generation quarks is thus very small, and so will be neglected. Moreover, the mixing between the SM quarks is given approximately by the usual CKM description. The flavour violating effects among the heavy quarks are then related to the mixing of the right-handed $SU(2)$ quark-doublet with the third generation right-handed quarks, as well as the mixing of the left-handed $SU(2)$ quark-singlet with the left-handed bottom-quark.

The mixing in the top sector must be very small to avoid a conflict with the $\mathcal{B}(b \to s\gamma)$ predictions [26]. We shall therefore assume, for simplicity, vanishing mixing in the top sector ($y_4 = 0$). The top-sector mass matrix is then diagonal, with $m_t = \frac{v}{\sqrt{2}}y_t$ and $m_\chi = M_1$.

Following [6] we take $y_5 = 0$ as well. The bottom-sector mass matrix, in the basis (b', ω', ξ'), is then given by

$$\lambda_d = \begin{pmatrix} Y_b & 0 & Y_3 \\ Y_2 & M_1 & 0 \\ 0 & 0 & M_2 \end{pmatrix} \qquad (27)$$

where $Y_i = \frac{v}{\sqrt{2}}y_i$, $i = b, 2, 3$. The phenomenologically interesting regime is $Y_b, Y_3 \ll Y_2, M_1, M_2$ [6]. Working to linear order in the small quantities Y_b/M_1 and Y_3/M_2, the left- and right-handed

mixing matrices are

$$U_d = \begin{pmatrix} c_L\tilde{c}_L & s_L & c_L\tilde{s}_L \\ -s_L & c_L & 0 \\ -\tilde{s}_L & 0 & \tilde{c}_L \end{pmatrix} \tag{28}$$

and

$$W_d = \begin{pmatrix} c_R & s_R & 0 \\ -s_R & c_R & 0 \\ 0 & 0 & 1 \end{pmatrix} \tag{29}$$

where $s_R = \sin\theta_R$, $s_L = \sin\theta_L$, and $\tilde{s}_L = \sin\tilde{\theta}_L$ are given by

$$\begin{aligned} s_R &= \frac{Y_2}{(Y_2^2 + M_1^2)^{1/2}}, \\ s_L &= \frac{Y_b Y_2}{(M_1^2 + Y_2^2)}, \\ \tilde{s}_L &= \frac{Y_3}{M_2}. \end{aligned} \tag{30}$$

Applying the mixing matrices to λ_d, the b-sector masses are

$$\begin{aligned} m_b &= Y_b \left(1 + \tfrac{Y_2^2}{M_1^2}\right)^{-1/2}, \\ m_\omega &= (M_1^2 + Y_2^2)^{1/2}, \qquad m_\xi = M_2. \end{aligned} \tag{31}$$

To obtain a good agreement between the predictions of the model and precision electroweak data the angle in the right-handed sector must be sizeable,

$$\tan\theta_R = Y_2/M_1 \simeq 0.7, \tag{32}$$

while $\tilde{s}_L$ should be small,

$$\sin\tilde{\theta}_L \simeq 0.09. \tag{33}$$

Note that Eq. (32) fixes s_L in terms of the b mass.

In this approximation, the relevant neutral currents read

$$\begin{aligned} \cos\theta_w J_Z^\mu &= \bar{b}_R\gamma^\mu b_R \left(-\frac{s_R^2}{2} + \frac{\sin^2\theta_W}{3}\right) \\ &+ \bar{\omega}_R\gamma^\mu\omega_R \left(-\frac{c_R^2}{2} + \frac{\sin^2\theta_W}{3}\right) - \left(\bar{b}_R\gamma^\mu\omega_R + h.c.\right)\frac{s_R c_R}{2} \\ &+ \bar{b}_L\gamma^\mu b_L \left(-\frac{\tilde{c}_R^2}{2} + \frac{\sin^2\theta_W}{3}\right) \\ &+ \bar{\xi}_L\gamma^\mu\xi_L \left(-\frac{\tilde{s}_L^2}{2} + \frac{\sin^2\theta_W}{3}\right) + \left(\bar{b}_L\gamma^\mu\xi_L + h.c.\right)\frac{\tilde{s}_L\tilde{c}_L}{2} \\ &+ \bar{\omega}_L\gamma^\mu\omega_L \left(-\frac{1}{2} + \frac{\sin^2\theta_W}{3}\right) + \bar{\xi}_R\gamma^\mu\xi_R\frac{\sin^2\theta_W}{3}. \end{aligned} \tag{34}$$

Within the same approximation, the charged currents read

$$\begin{aligned} J^{\mu}_{W^+} &= \bar{t}_L \gamma^{\mu} \left(\tilde{c}_L b_L + s_L \omega_L + \tilde{s}_L \xi_L \right) \\ &+ \bar{\chi}_L \gamma^{\mu} \left(\omega_L - s_L b_L \right) \\ &+ \bar{\chi}_R \gamma^{\mu} \left(c_R \omega_R - s_R b_R \right), \end{aligned} \tag{35}$$

where we have neglected terms of order m_b^2/M_1^2.

3.2 Higgs Couplings

One of the most important immediate goals of high energy physics is to understand the mechanism of electroweak symmetry breaking. In the Standard Model and its supersymmetric extensions, this symmetry is broken spontaneously through the vacuum expectation value of one or more scalar Higgs bosons. The same is true for the model under study and it is therefore quite relevant to understand the possible modification of the Higgs boson search channels at the Tevatron and the LHC.

In addition to introducing new sources of flavour mixing, mirror quarks also modify the couplings to the Higgs. The Dirac mass terms for the mirror quarks mean that the Higgs-quark couplings need no longer be flavour diagonal in the basis of mass eigenstates, nor be proportional to the quark masses. We find that the coupling of the Higgs to the b quark is reduced relative to the SM. This, along with the contribution of the heavy quarks in loops, has interesting consequences for the detection of the Higgs.

As in the previous section, we will assume that the mirror quarks mix almost exclusively with the third generation quarks and take $y_4, y_5 \approx 0$. This implies that the only Higgs-quark coupling that is significantly modified from the SM is that of the b-quark. The relevant terms in the Lagrangian are therefore

$$\mathscr{L} \supset -(y_b \bar{Q}'_L + y_2 \bar{\Psi}'_L) b'_R \Phi - y_3 \bar{Q}'_L \xi'_R \Phi - M_1 \bar{\Psi}'_L \Psi'_R - M_1 \bar{\xi}'_L \xi'_R + (h.c.). \tag{36}$$

After symmetry breaking $\Phi = \frac{1}{\sqrt{2}} \binom{0}{v+h}$ in the unitary gauge. These couplings can then be written as

$$\mathscr{L} \supset -\bar{d}'_L \left(M_b + h N_b \right) d'_R + (h.c.) \tag{37}$$

with $d'_{L,R} = \left(b'_{L,R}, \omega'_{L,R}, \xi'_{L,R} \right)^t$, and

$$N_b = \begin{pmatrix} Y_b & 0 & Y_3 \\ Y_2 & 0 & 0 \\ 0 & 0 & 0 \end{pmatrix}. \tag{38}$$

Transforming to the mass eigenstate basis, the Higgs couplings become

$$\begin{aligned}\mathscr{L} \supset & -c_R^2 \frac{m_b}{v} h \bar{b}_L b_R - s_R^2 \frac{m_\omega}{v} h \bar{\omega}_L \omega_R \\ & - s_R c_R h \frac{m_b}{v} \bar{b}_L \omega_R - s_R c_R h \frac{m_\omega}{v} \bar{\omega}_L b_R \\ & - \frac{m_\xi \tilde{s}_L}{v} h \left(\bar{b}_L + \tilde{s}_L \bar{\xi}_L \right) \xi_R \ + \ (h.c.).\end{aligned} \tag{39}$$

Using the value $\tan\theta_R = Y_2/M_1 \simeq 0.7$ favoured by the model, we find that the hbb coupling is reduced by a factor of $c_R^2 \sim 2/3$.

4 Higgs Phenomenology

4.1 Higgs Production and Decay

This scenario modifies the phenomenology of the Higgs in two ways. First, by reducing the hbb coupling by a factor of c_R^2, the partial width $\Gamma(h \to \bar{b}b)$ is attenuated by the square of this factor, $c_R^4 \sim 4/9$. Since this channel is dominant for Higgs masses below $m_h \simeq 130$ GeV, the reduction of the partial width for this mode increases the branching fractions of the other modes in this range. Secondly, ω quark loop effects increase the partial width $\Gamma(h \to gg)$. This increases both the branching fraction of this mode, and the Higgs production cross-section by gluon fusion.

Let us consider the effect of the ω quark in a bit more detail. The presence of this quark in a loop connecting the Higgs to two gluons modifies the $h \to gg$ partial width. Neglecting light quark contributions, and keeping only the effects of the dominant Yukawa coupling y_2, the partial width becomes

$$\Gamma(h \to gg) = \frac{\alpha \alpha_s^2}{128 \pi^2 \sin^2\theta_w} \left(\frac{m_h^3}{M_W^2} \right) \left| F_{1/2}(\tau_t) + s_R^2 F_{1/2}(\tau_\omega) \right|^2 \tag{40}$$

where the function $F_{1/2}(\tau_q)$ is given by [27]

$$F_{1/2} = -2\tau_q [1 + (1 - \tau_q) f(\tau)], \tag{41}$$

with $\tau_q = 4(\frac{m_q}{m_h})^2$ and

$$f(\tau) = \begin{cases} [\sin^{-1}(1/\sqrt{\tau})]^2; & \tau \geq 1 \\ -\frac{1}{4}[\ln(\eta_+/\eta_-) - i\pi]^2; & \tau < 1; \quad \eta_\pm = 1 \pm \sqrt{1-\tau}. \end{cases} \tag{42}$$

The corresponding expression in the SM is obtained by setting $s_R = 0$. Since the new term interferes constructively, the effect is to increase the decay width. While the $h \to gg$ mode isn't directly observable at hadron colliders, this decay width is nevertheless important because it determines the cross-section for Higgs production by gluon fusion; $\sigma(gg \to h) \propto \Gamma(h \to gg)$, up to soft gluonic effects. The $h \to \gamma\gamma$ decay width is similarly modified by an ω loop. In this case, the new contribution interferes destructively with the SM terms, the dominant parts of which come from W and Goldstone boson loops. However, the change in $\Gamma(h \to \gamma\gamma)$ is very small for any reasonable input parameter values. Figure 3 shows the dominant Higgs decay branching ratios in the model under study. Additional NLO corrections to the $h \to gg$ mode were included as well, following [28].

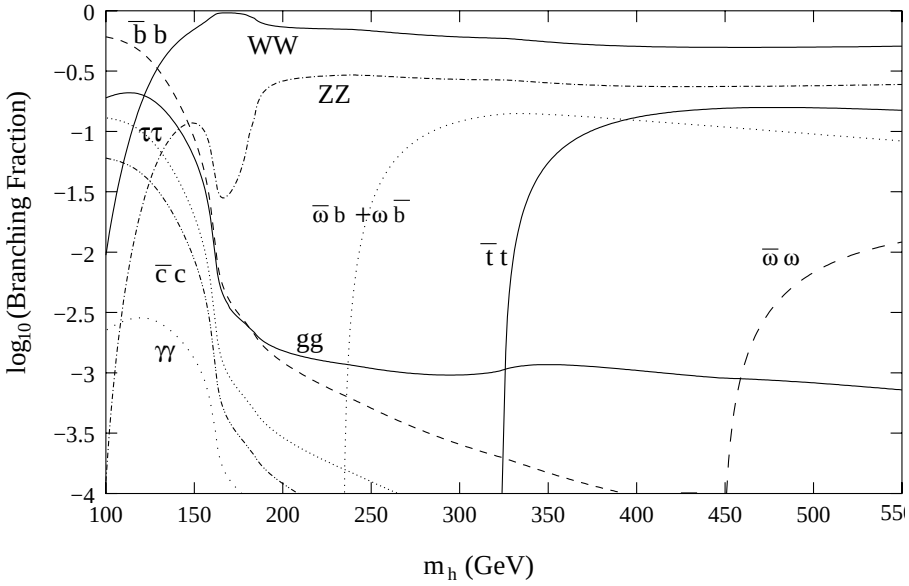

Figure 3: Higgs Branching Ratios with Mirror Quarks, for $m_\omega = 250$ GeV and $Y_2/M_1 = 0.7$.

Figures 4 and 5 show the enhancement of a few Higgs discovery modes relative to the SM, which is mostly due to the increase in the gluon fusion cross-section. For low Higgs masses, $m_h \lesssim 150$ GeV, there is an additional enhancement of certain modes as a result of the decrease in the $h \to \bar{b}b$ branching ratio. It should be noted, however, that such low Higgs masses worsen the fit to the precision electroweak data in this model.

If the Higgs mass exceeds 150 GeV the process $h \to VV$, where V is a real or virtual vector boson, becomes the primary Higgs discovery mode at both the Tevatron and the LHC [29, 30]. The inclusive modes are enhanced by the increase in gluon fusion, while modes in which the

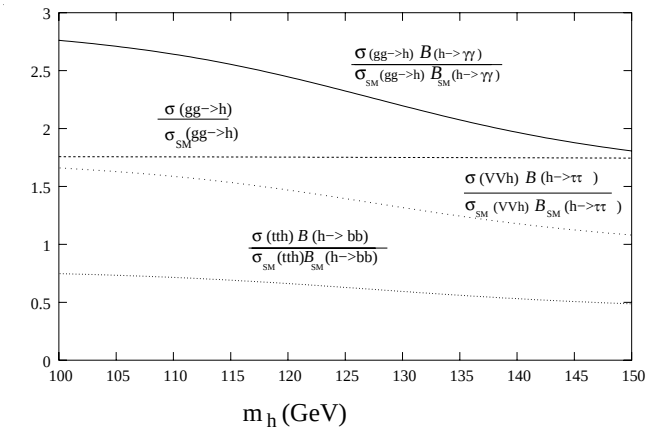

Figure 4: Enhancement of low mass Higgs production and detection modes for $m_\omega = 250$ GeV, $Y_2/M_1 = 0.7$.

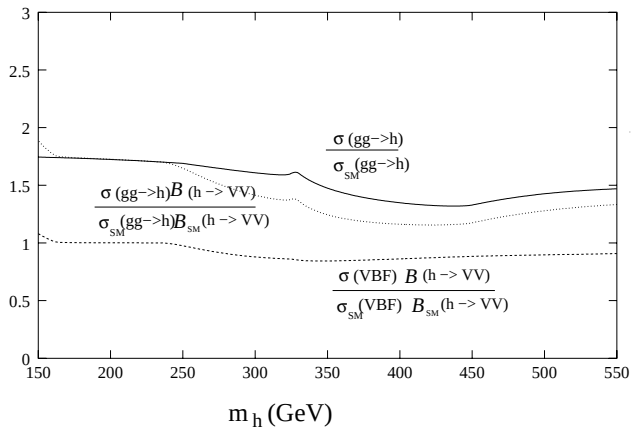

Figure 5: Enhancement of intermediate mass Higgs modes for $m_\omega = 250$ GeV, $Y_2/M_1 = 0.7$.

Higgs is produced by other means, such as vector boson fusion, are very slightly attenuated due to Higgs decays into mirror quarks.

4.2 Higgs Searches at the Tevatron and the LHC

The enhancement of Higgs detection signals decreases the collider luminosity needed to find the Higgs. We have translated the above results into collider units using detector simulation results from [31, 32, 33] for the Tevatron, and [33, 34] for the LHC. Figure 6 shows the minimum luminosity per detector (with CDF and D$\emptyset$ data combined) needed for a 3-σ signal at the Tevatron. Figure 7 shows the luminosity needed for a 5-σ discovery at the LHC. All channels displayed in this plot are for CMS alone except for the WW and ZZ modes, which are for ATLAS. These plots correspond to inclusive searches unless stated otherwise: $VV \to h \to X$ denotes weak boson fusion channels, while $\bar{t}th \to X$ and $W/Zh \to X$ denote associated production channels. For the inclusive channels, we have assumed that gluon fusion accounts for 80% of the total Higgs production.

The model significantly improves the likelihood of observing the Higgs at the Tevatron for a Higgs mass between 120 and 180 GeV. Note that $gg \to h \to \tau^+\tau^-$ becomes the dominant discovery channel at the Tevatron collider in the low Higgs mass region.

The predictions of the model for the LHC are less dramatic, although the improvement in the $gg \to h \to \gamma\gamma$ process will make a light Higgs much easier to see. For intermediate Higgs masses, the inclusive $h \to WW$ channel becomes competitive with the $VV \to h \to WW$

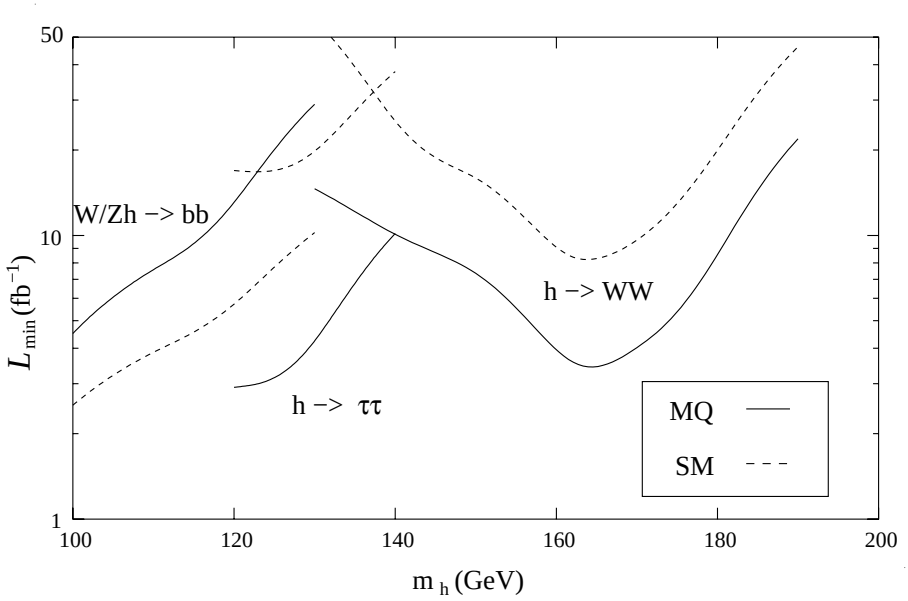

Figure 6: Minimum luminosity needed for a 3-σ Higgs signal at the Tevatron for $m_\omega = 250$ GeV, $Y_2/M_1 = 0.7$.

channel. For masses larger than the ones displayed in the Figure 7, searches for the Higgs at the LHC can proceed via the golden mode $h \to ZZ$.

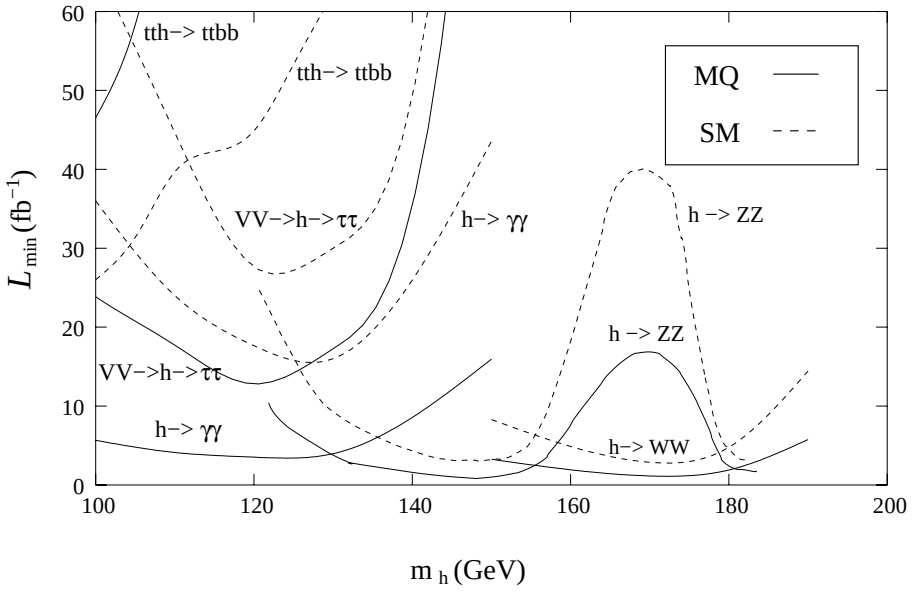

Figure 7: Minimum luminosity needed for a 5-σ Higgs discovery at the LHC for $m_\omega = 250$ GeV, $Y_2/M_1 = 0.7$.

5 Mirror Quark Collider Signals

If the model is to improve the electroweak fits, the mirror quarks must not be too heavy. In particular, this requires $m_\chi \lesssim 250$ GeV, which (using (17)) implies $m_\omega \lesssim 300$ GeV as well. On the other hand, m_ξ is largely unconstrained. These relatively low masses suggest that the Tevatron may be able to see mirror quarks by the end of Run II. Previous searches for exotic quarks have concentrated on a possible fourth generation b' quark. In the most recent of these, CDF has put a lower bound on the b' mass of $m_{b'} > 199$ GeV[35], provided the branching ratio $b' \to bZ$ is 100%. This bound is relevant to our model as well.

At the Tevatron, mirror quarks are produced mostly by $\bar{q}q$ annihilation, with a smaller contribution from gluon fusion. Previous calculations of the top-quark pair-production cross-section apply to mirror quarks as well. These indicate $\sigma_{\bar{q}q} \simeq 3.0 - 0.5$ pb, for $m_q = 200 - 300$ GeV at the centre of mass energy $\sqrt{s} = 2.0$ TeV[36, 37]. This is small, but comparable to the top production cross section in Run I, $\sigma_{\bar{t}t} = 6.1 \pm 1.1$ pb, where we have averaged the results of DØ and CDF[17].

The up-type χ quark is most strongly constrained in the model. It decays almost entirely by $\chi_R \to b_R W$ due to a large tree-level right-handed W coupling, Eq. (35). This will produce a signature very similar to that of the top quark. Indeed, top quark decays present a nearly irreducible background. Searching for the χ therefore reduces largely to a counting experiment in which one compares the number of measured top events to the number expected. Searches at Run I of the Tevatron have already put interesting limits on m_χ since the top production cross-section measured there agrees well with SM predictions[37] (See, however, the comments in [38].)

In order to make a quantitative estimate of the present bound on a possible sequential top quark, we conservatively assume equal acceptance and detection rates for both χ and top events. The fraction of χ events in the top sample will be 40-10% for $200 < m_\chi < 250$ GeV. (In practice, the detection efficiency for χ's will be slightly better since the b-tagging efficiency improves with jet P_T.) Comparing the Run I value for the top production cross-section with the theoretical prediction [37], we get that the cross-section for any new sequential top quark should be lower than 2.9 pb, at the 2-σ level. This method, based just on counting, leads to a bound of about

$$m_\chi \gtrsim 200 \text{ GeV}. \tag{43}$$

This in turn implies $m_\omega \gtrsim 250$ GeV, well in excess of the b' bound from [35].

At Run II, the goal is to determine the top production cross section to an accuracy of 7–9% [39] with a few fb^{-1} of data. Assuming that this goal is achieved, and considering that the uncertainty is mostly due to systematic effects (in particular, the proper determination of the b-tagging efficiency) and therefore weakly dependent on small luminosity variations, the Tevatron Run II will be sensitive enough to rule out the presence of a sequential top quark with a mass smaller than 230 GeV. This will imply an indirect bound on $m_\omega > 285$ GeV. On the other hand, the Tevatron might see evidence of a χ quark with mass smaller than 220 GeV at the 3-σ level.

That the $\chi \to bW$ vertex is $(V+A)$, Eq. (35), makes the χ somewhat easier to find. This is because the W^+'s emitted in $\chi_R \to b_R W^+$ have positive or zero helicity, whereas those from $t_L \to b_L W^+$ have negative or zero helicity [3]. Leptons emitted by positive helicity W's tend to be harder than those from longitudinal or negative helicity W's. Thus, a slightly higher lepton P_T cut will increase the relative acceptance of χ's, although the improvement will be small since the majority of W's emitted are longitudinal. CDF has looked for positive helicity W's in top decays. They find a positive helicity fraction of $\mathcal{F}_+ = 0.11 \pm 0.15$[40], consistent with both the SM, and a χ of mass above about 200–250 GeV, for which we predict a value of $\mathcal{F}_+ \lesssim 0.08$–$0.02$ [41].

Run II at the Tevatron will also cover part of the mass range of the ω quark by direct searches for this particle. The strong ωb mixing leads to tree-level $bZ\omega$ and $bh\omega$ vertices, Eqs. (34),(39), with the same $\mathcal{O}(1)$ flavour-mixing factors. The dominant decay modes are thus $\omega_R \to b_R Z$, and $\omega_R \to b_L h$ provided the Higgs isn't heavier than the ω. Other modes are suppressed by loops, small flavour-mixing factors, and in the case of $\omega \to \chi W$, phase space. Indeed, this decay is forbidden for almost all of the model parameter space consistent with precision electroweak data[6]. If the Higgs is heavier than the ω, the CDF bound applies directly to $\bar{\omega}\omega \to \bar{b}bZZ$ modes and constrains the ω mass to be greater than 199 GeV.

Things are more interesting if the Higgs is lighter than the ω. In this case, the ratio of the decay widths of the Higgs and Z modes is [42]

$$\frac{\Gamma(\omega \to bh)}{\Gamma(\omega \to bZ)} = \frac{(1-r_h)^2}{(1-r_Z)^2(1+2r_Z)} \tag{44}$$

where $r_h = (m_h/m_\omega)^2$, $r_Z = (M_Z/m_\omega)^2$. Figure 8 shows the branching ratios for these modes for a Higgs mass of 170 GeV. In their b' search, CDF looked for $\bar{b}'b' \to \bar{b}bZZ$ events in which

[3] Correspondingly, the W^-'s emitted in the charge conjugate decays have negative or zero helicity for a $(V+A)$ vertex, and positive or zero helicity for a $(V-A)$ vertex. We shall refer to both positive helicity W^+'s and negative helicity W^-'s as "positive helicity" W's, and so on.

one Z decayed into jets while the other decayed into a pair of high transverse momentum (P_T) leptons[35]. They only accepted events in which the reconstructed mass of the lepton pair lay within the range 75-105 GeV and at least two jets were tagged as b's. For low Higgs masses, below 150 GeV, this search strategy is sensitive to both $\omega\omega \to bZbZ$ and $\omega\omega \to bZbh$ events, since in the latter, the Higgs decays predominantly into a $\bar{b}b$ pair which mimics the hadronic decay of a Z. This also lends itself to modifying the search strategy to include four b-tags [42]. Even more search strategies become possible if the Higgs mass exceeds 150 GeV as favoured by the model. Such massive Higgs bosons decay mostly into WW pairs (see Figure 3) so for instance, $\omega\omega \to bZbh$ could be distinguished by looking for events with four jets, at least two of which are b-tagged, accompanied by a pair of high P_T leptons and large missing E_T.

In order to estimate the possibility of observing an ω quark at the Tevatron using the CDF b' search strategy, we shall assume that the Higgs mass is $m_h = 170$ GeV, and that this search strategy has no sensitivity to the $\omega \to bh$ modes and a detection efficiency of 13% (as in Run I for large $m_{b'}$). The most important background comes from Z^0 events associated with hadronic jets. To reduce the background, one can impose a cut on the total transverse energy of the jets [35]. For $m_\omega > 250$ GeV, a cut of $\sum E_T > 150$ GeV will eliminate most of the background without reducing the signal in a significant way. The number of observable signal events scales with the luminosity and is approximately equal to

$$N_{\omega\bar{\omega}} \simeq 1.5 - 7.0 \;\; \mathcal{L}[\text{fb}^{-1}] \,, \tag{45}$$

for an ω mass varying from 300 GeV to 250 GeV. Due to the smallness of the background, a simple requirement for evidence of a signal is that at least five events be observed. Therefore the Tevatron Run II should cover the whole mass range of the model, $m_\omega < 300$ GeV, if the luminosity is above 4 fb $^{-1}$. For a luminosity of 2 fb^{-1}, a signal may be observed up to masses of about 280 GeV.

The isosinglet ξ decays predominantly by $\xi_L \to b_L Z$, $\xi_L \to t_L W$, and $\xi_R \to b_L h$ (see Eqs. (34),(35) and (39)). All three of these go at tree level. Figure 9 shows the corresponding branching ratios for these decays. The $\xi \to bZ$ mode is dominant for $m_\xi \lesssim 400$ GeV, although the $\xi \to tW$ quickly becomes important above the tW-production threshold[43]. For relatively light ξ's, of mass less than 250 GeV, the search strategies are similar to those for the ω. The CDF b' search is thus sensitive to a light ξ. Their b' mass bound also applies in this case, although this limit may be weakened somewhat depending on the mass of the Higgs.

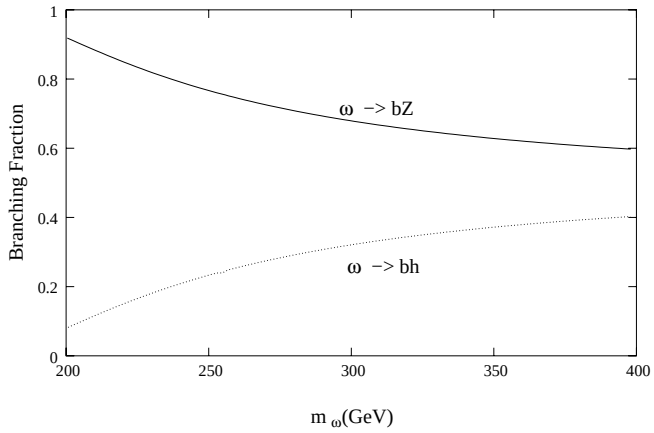

Figure 8: Branching ratios for decays of the ω quark with $m_h = 170$ GeV.

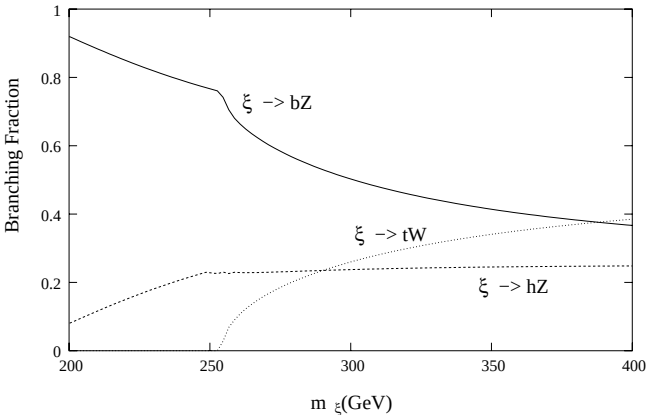

Figure 9: Branching ratios for decays of the ξ quark with $m_h = 170$ GeV.

6 CP-violation in $B^0 \to \phi K_s$ Decays

The value of the CP-violation parameter $\sin(2\beta)$ measured in $B^0 \to \phi K_s$ decays appears to disagree with the value extracted from $B^0 \to J/\psi K_s$ decays: [44, 45, 46]

$$\sin(2\beta) = \begin{cases} +0.735 \pm 0.054; & B^0 \to J/\psi K_s \\ -0.39 \pm 0.41; & B^0 \to \phi K_s \end{cases} \tag{46}$$

This discrepancy is particularly interesting because the $B \to \phi K_s$ mode is loop mediated, making it much more sensitive to new physics than the $B \to J/\psi K_s$ mode, which goes at tree-level. We investigate whether this discrepancy can be explained by the FCNC's which arise in the model.

It is not $\sin(2\beta)$ that is measured directly, but rather the time-dependent CP asymmetry $a_{CP}(t)$. For decays of the $B^0(= \bar{b}d)$ meson into a CP eigenstate f, this is defined to be [47]

$$\begin{aligned} a_{CP}^f(t) &:= \frac{\Gamma(B^0(t) \to f) - \Gamma(\bar{B}^0(t) \to f)}{\Gamma(B^0(t) \to f) + \Gamma(\bar{B}^0(t) \to f)} \\ &= \mathcal{C}_f \cos(\Delta M t) - \mathcal{S}_f \sin(\Delta M t) \end{aligned} \tag{47}$$

where ΔM is the mass difference between the mass eigenstates, and $\mathcal{S}_f$, $\mathcal{C}_f$ are given by

$$\mathcal{C}_f = \frac{1-|\xi_f|^2}{1+|\xi_f|^2}, \qquad \mathcal{S}_f = -\frac{2Im\xi_f}{1+|\xi_f|^2}, \tag{48}$$

with ξ_f given by (for the B_d^0 system)

$$\xi_f \equiv e^{-2i\beta} \frac{A(\bar{B}^0 \to \bar{f})}{A(B^0 \to f)}. \tag{49}$$

In the SM, the $\bar{B} \to \phi \bar{K}_s$ amplitude has the form $\bar{A} = \lambda_t A_0$, where A_0 is CP-invariant and $\lambda_t = V_{CKM}^{ts*} V_{CKM}^{tb}$. The phase of λ_t is very small [47], so to a good approximation $\mathcal{C}_{\phi K} = 0$, and $\mathcal{S}_{\phi K} = \sin(2\beta)$. This result applies to the $B \to J/\psi K_s$ mode as well. For this reason, the values of $\mathcal{S}_f$ measured in the ϕK_s and $J/\psi K_s$ modes are sometimes quoted as $\sin(2\beta)$, as we have done in (46).

Physics beyond the SM can change the values of $\mathcal{S}_{\phi K_s}$ and $\mathcal{S}_{J/\psi K_s}$ by adding additional CP-violating terms to the decay amplitudes. We have investigated whether the new tree-level FCNC Z-couplings

$$J_Z^\mu \supset \frac{1}{2\cos\theta_w} \left(\bar{s}_L \gamma^\mu V_d^{sb} b_L - \bar{s}_R \gamma^\mu \tilde{V}_d^{sb} b_R \right) + (h.c.) \tag{50}$$

can explain the apparent difference between $\mathcal{S}_{\phi K}$ and $\mathcal{S}_{J/\psi K_s}$. To simplify the analysis, we have assumed that the mixing of the mirror quarks with the SM quarks (other than the b) is very small. In particular, we have neglected all right-handed W couplings and all FCNC couplings other than those connecting the b and s quarks. $|V^{sb}|$ and $|\tilde{V}^{sb}|$ will also be treated as small parameters whose size we will bound below. These assumptions imply that the three generation CKM description of flavour mixing in the SM is correct up to small modifications, and that we can ignore the loop contributions of mirror quarks to the effective sb vertex.

6.1 Constraints from Semi-Leptonic Decays

The strongest constraints on these couplings come from semileptonic $b \to s$ modes [48]. At energies much below M_Z, the SM decay amplitudes can be written as the matrix elements of an effective Hamiltonian;

$$\mathcal{H}_{eff} = \mathcal{H}_{eff}(b \to s\gamma) - \frac{G_F}{\sqrt{2}} \lambda_t (C_{9_V}^{SM} Q_{9_V} + C_{10_A}^{SM} Q_{10_A}), \tag{51}$$

where $Q_{9_V} = (\bar{s}b)_{(V-A)}(\bar{l}l)_V$, and $Q_{10_A} = (\bar{s}b)_{(V-A)}(\bar{l}l)_A$ are four-quark operators, $\lambda_t = V_{CKM}^{ts*} V_{CKM}^{tb}$, and $l = \mu, e$. (See [49] for a definition of $\mathcal{H}_{eff}(b \to s\gamma)$.) The FCNC couplings contribute to Q_{9_V} and Q_{10_A}, and generate the new $(V+A)$ operators $Q'_{9_V} = (\bar{s}b)_{(V+A)}(\bar{l}l)_V$, and $Q'_{10_A} = (\bar{s}b)_{(V+A)}(\bar{l}l)_A$.

We neglect the contribution of mirror quarks to $\mathcal{H}_{eff}(b \to s\gamma)$, since these only arise from loops, that become negligible for $y_4 = 0$, contrary to the dominant tree-level effects included in our analysis. The effective Hamiltonian thus becomes

$$\mathcal{H}_{eff} = \mathcal{H}_{eff}(b \to s\gamma) - \frac{G_F}{\sqrt{2}} \lambda_t \left(C_9 Q_{9_V} + C_{10} Q_{10_A} + C'_9 Q'_{9_V} + C'_{10} Q'_{10_A} \right). \tag{52}$$

In terms of $\eta := \frac{V_d^{sb}}{\lambda_t}$ and $\eta' := -\frac{\tilde{V}_d^{sb}}{\lambda_t}$, the Wilson coefficients are now given by

$$\begin{array}{rclcrcl} C_{9_V} & = & C_{9_V}^{SM} + (\frac{1}{2} - 2\sin^2\theta_w)\eta, & & C'_{9_V} & = & (\frac{1}{2} - 2\sin^2\theta_w)\eta', \\ C_{10_A} & = & C_{10_A}^{SM} - \frac{1}{2}\eta, & & C'_{10_A} & = & -\frac{1}{2}\eta'. \end{array} \tag{53}$$

Since $\frac{1}{2} - 2\sin^2\theta_w \simeq 0.05$, to a good approximation we need only consider the shift in the C_{10_A} coefficients. We have examined the effect of modifying the C_{10_A} coefficients on the branching ratios of the inclusive $B \to X_s l^+ l^-$ mode, as well as the two exclusive $B \to K l^+ l^-$ and $B \to K^* l^+ l^-$ decays.

The constraint on $b \to s$ FCNC's from the $B \to X_s l^+ l^-$ mode has been considered previously (*e.g.*[49, 50, 51]). We repeat the analysis for this particular model using updated input values. From [49], modified to include the new $(V + A)$ operators and neglecting lepton masses, the shift in the branching ratio relative to the SM is

$$\begin{aligned} \Delta\mathcal{B}^{X_s} &= \mathcal{B} - \mathcal{B}^{SM} \\ &= \frac{\alpha^2}{8\pi^2 f(z)\kappa(z)} \left|\frac{V_{ts}}{V_{cb}}\right|^2 \left(|\tilde{C}_{10_A}|^2 + |\tilde{C}'_{10_A}|^2 - |\tilde{C}^{SM}_{10_A}|^2\right) \mathcal{B}(b \to ce\bar{\nu}), \end{aligned} \tag{54}$$

where $\tilde{C}_i := \frac{2\pi}{\alpha} C_i$, $f(z) = 0.54 \pm 0.04$ is a phase space factor, $\kappa = 0.879 \pm 0.002$ is a QCD correction, and $\mathcal{B}(b \to ce\bar{\nu}) = 0.109 \pm 0.005$. We have also taken $C_{10_A}^{SM} = -\frac{Y_0(x_t)}{\sin^2\theta_w} \simeq -4.2$, $\alpha^{-1}(m_b) = 129$, and $\left|\frac{V_{ts}}{V_{cb}}\right|^2 = 1$ in our analysis. The measured branching ratio and the SM prediction for this mode are listed in Table 6.1, as is the 2-σ allowed shift in the branching ratio based on these values.

Mode	$\mathcal{B}^{exp}(10^{-6})$	$\mathcal{B}^{SM}(10^{-6})$	2-σ Allowed Range (10^{-6})
$B \to X_s l^+ l^-$	$6.1 \pm 1.4^{+1.4}_{-1.1}$ [53]	5.5 ± 0.6 [54]	-3.6 $< \Delta\mathcal{B}^{X_s} <$ 4.8
$B \to K l^+ l^-$	$0.76^{+0.19}_{-0.18}$ [55, 56]	0.35 ± 0.12 [54]	$-0.09 < \Delta\mathcal{B}^{K} < 0.91$
$B \to K^* l^+ l^-$	$1.68^{+0.68}_{-0.58} \pm 0.28$ [56]	1.39 ± 0.31 [54]	$-1.3 < \Delta\mathcal{B}^{K^*} < 2.1$

Table 1: Experimental inputs and SM predictions. All errors were combined in quadrature, and the SM predictions were averaged over μ and e modes.

The inclusive modes $B \to K l^+ l^-$ and $B \to K^* l^+ l^-$ have been considered in [51, 52]. The result for the latter mode, neglecting lepton masses, is [51]

$$\begin{aligned} \Delta\mathcal{B}^{K^*} &= (4.1^{+1.0}_{-0.7}) \times 10^{-8} \left(|\tilde{C}_{10_A} - \tilde{C}'_{10_A}|^2 - |\tilde{C}^{SM}_{10_A}|^2\right) \\ &\quad + (0.9^{+0.4}_{-0.2}) \times 10^{-8} \left(|\tilde{C}_{10_A} + \tilde{C}'_{10_A}|^2 - |\tilde{C}^{SM}_{10_A}|^2\right). \end{aligned} \tag{55}$$

Table 6.1 lists the experimental values, the theoretical SM prediction, and the corresponding 2-σ allowed range for $\Delta\mathcal{B}^{K*}$.

For the $B \to K l^+ l^-$ mode, the shift in the branching ratio is [51]

$$\Delta\mathcal{B}^K = \frac{G_F^2 \alpha^2 m_B^5}{1536\pi^5} \tau_B |\lambda_t|^2 I \left(|\tilde{C}_{10_A} + \tilde{C}'_{10_A}|^2 - |\tilde{C}^{SM}_{10_A}|^2 \right), \tag{56}$$

where $\tau_B = 1.60 \pm 0.05$ ps is the total B lifetime, and I is an integral of form factors. Explicitly, $I = \int_{\hat{s}_0}^{\hat{s}_1} d\hat{s} \lambda_K^{3/2}(\hat{s}) f_+^2(\hat{s})$, where $0 \simeq \frac{4m_l^2}{m_B^2} \leq \hat{s} \leq \frac{(m_B - m_K)^2}{m_B^2}$, and $\lambda_K(\hat{s}) = 1 + r_K^2 + \hat{s}^2 - 2\hat{s} - 2r_K\hat{s}$ with $r_K = (m_K/m_B)^2$. We have evaluated the integral I numerically using the form factors in [52], and find $I = (0.056^{+0.015}_{-0.09})$. Again, table 6.1 lists the relevant input data.

Figure 10 shows the η and η' values consistent with all three semileptonic decay mode constraints taken at the 2-σ level. Note that points within the two regions are correlated.

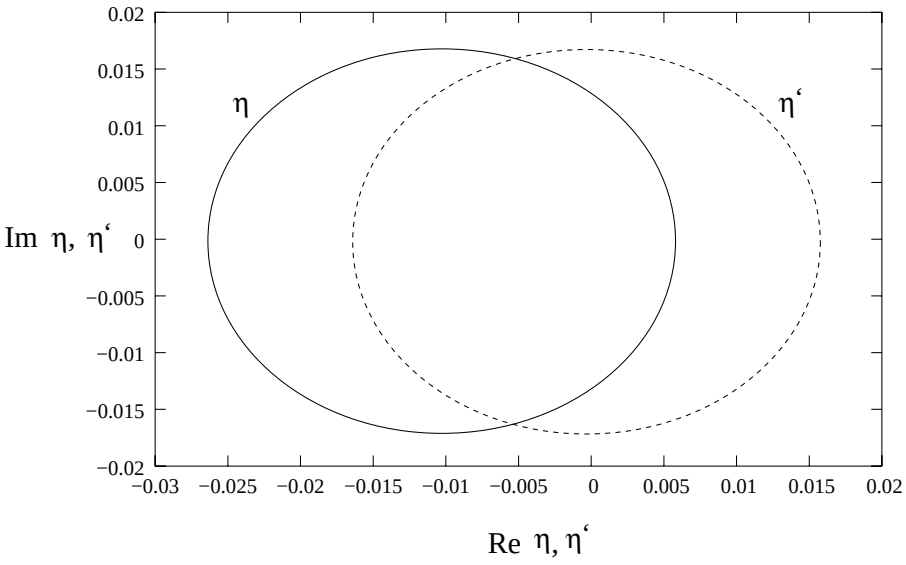

Figure 10: 2-σ allowed ranges of η and η'.

6.2 Range of $\mathcal{S}_{\phi K}$

As for the semi-leptonic modes, the non-leptonic $B \to \phi K_s$ decay amplitude can be written in terms of an effective Hamiltonian. In the SM, this is given by [57]

$$\mathcal{H}_{eff}^{SM} = \frac{G_F}{\sqrt{2}} \left[\lambda_u (C_1 Q_1^u + C_2 Q_2^u) + \lambda_c (C_1 Q_1^c + C_2 Q_2^c) - \lambda_t \sum_{i=3}^{10} C_i Q_i \right], \tag{57}$$

where $\lambda_q = V_{CKM}^{qs^*} V_{CKM}^{qb}$ are products of CKM factors, $Q_i(\mu)$ are four-fermion operators, $C_i(\mu)$ are the Wilson coefficients, and μ is the renormalization scale.[4] The operators $Q_1, Q_2, Q_3, \ldots Q_6$, and $Q_7 \ldots Q_{10}$ are the usual SM current-current, QCD penguin, and electroweak (EW) penguin operators respectively, as defined in [57]. Note that the four-quark operators Q_9 and Q_{10} are different from the semi-leptonic operators Q_{9_V} and Q_{10_A} considered above.

If we include the FCNC couplings from the mirror quarks, the tree-level contribution to $\mathcal{H}_{eff}$ at scale M_W is

$$\Delta\mathcal{H}_{eff} = +\frac{G_F}{\sqrt{2}}\lambda_t \left[\eta(\bar{s}b)_{(V-A)} \sum_q g_{R,L}^q (\bar{q}q)_{(V\pm A)} + \eta'(\bar{s}b)_{(V+A)} \sum_q g_{R,L}^q (\bar{q}q)_{(V\pm A)}\right] \tag{58}$$

where the sum runs over $q = u, d, s, c, b$, $g_{R,L}^q = (T_3 - e_q \sin^2\theta_w)$ is the $Z(\bar{q}q)_{L,R}$ coupling, and $\eta = \frac{V_d^{sb}}{\lambda_t}$ and $\eta' = -\frac{\tilde{V}_d^{sb}}{\lambda_t}$ are the same as above. The first operator, multiplied by η, can be written as a linear combination of $Q_3, \ldots, Q_{10}$. The second operator, multiplied by η', has no SM counterpart. We introduce a new "$(V+A)$" operator basis $Q'_1, \ldots, Q'_{10}$ related to $Q_1, \ldots, Q_{10}$ by the interchange $(V-A) \leftrightarrow (V+A)$ wherever these appear.

We incorporate the new $(V-A)$ operator contribution by modifying the Wilson coefficients at scale M_W. The changes are

$$\begin{aligned}
C_3^{SM}(M_W) &\rightarrow C_3^{SM}(M_W) + \frac{1}{6}\eta, \\
C_7^{SM}(M_W) &\rightarrow C_7^{SM}(M_W) + \frac{2}{3}\sin^2\theta_w\eta, \\
C_9^{SM}(M_W) &\rightarrow C_9^{SM}(M_W) - \frac{2}{3}(1-\sin^2\theta_w)\eta.
\end{aligned} \tag{59}$$

For the $(V+A)$ operators, $\left(C_i^{SM}\right)'(M_W) = 0$, while the FCNC contribution gives

$$\begin{aligned}
C'_5(M_W) &= \frac{1}{6}\eta', \\
C'_7(M_W) &= -\frac{2}{3}(1-\sin^2\theta_w)\eta', \\
C'_9(M_W) &= \frac{2}{3}\sin^2\theta_w\eta',
\end{aligned} \tag{60}$$

with all others zero.

The RG evolution of these operators proceeds much like in the SM since the $(V-A)$ and $(V+A)$ operators evolve independently. The anomalous dimension matrix that determines

[4] In writing $\mathcal{H}_{eff}$ in this form, we have made use of $\lambda_u + \lambda_c + \lambda_t \simeq 1$. This is also approximately true when mirror quarks are included.

running of both the $(V-A)$ and the $(V+A)$ operators is the same as in the SM. This follows from our definition of the $(V+A)$ operators, and the fact that these are renormalized by parity-invariant gauge interactions. We calculated the Wilson coefficients at scale $\mu = 2.5, 5.0$ GeV at one-loop order in both the QCD and QED corrections using the results of [58]. To this order, the corresponding initial values of the Wilson coefficients are taken at tree-level in the QCD corrections, although we have included the one-loop electroweak corrections which give a large contribution to $C_9(M_Z)$. (This agrees with the conventions of [57, 58, 59].)

Hadronic matrix elements for the $B \to \phi K_s$ transition at scale $\mu = 2.5, 5.0$ GeV were estimated using factorization. Following [60, 61], the amplitude is given by

$$A(\bar{B} \to \phi \bar{K}) = A_0 \lambda_t \left[a_3 + a_4 + a_5 - \frac{1}{2}(a_7 + a_9 + a_{10}) - \frac{1}{2}(a'_7 + a'_9 + a'_{10}) \right] \tag{61}$$

where $A_0 = -\sqrt{2} G_F f_\phi m_\phi F_1^{BK}(m_\phi^2)(\epsilon^* \cdot p_K)$ is a CP-invariant product of form factors and constants, and the a_i are functions of the Wilson coefficients. To leading order, they are [60]: $a_{2i-1} = C_{2i-1} + \frac{1}{N_{eff}} C_{2i}$, and $a_{2i} = C_{2i} + \frac{1}{N_{eff}} C_{2i-1}$, where N_{eff} is an effective number of colours. In writing (61), we have neglected annihilation contributions which may be significant [61].

The a_i coefficients were calculated numerically by taking as input the 2-σ allowed values of η and η' from the previous section, and running the Wilson coefficients down to $\mu = 2.5, 5.0$ GeV. From these we calculate $\mathcal{S}_{\phi K}$, and the $B \to \phi K_s$ branching ratio. This helps to reduce the theoretical uncertainty due to the sensitivity of the amplitude to variations of N_{eff}. Using (61) and the input parameters $f_\phi = 0.233$ GeV, $F_1^{BK} = 0.39 \pm 0.03$, $m_\phi = 1019.4$ MeV, $m_K = 497.7$ MeV, $m_B = 5279.3$ MeV, $\tau_{B^0} = 1.54 \pm 0.02$ ps, $|\lambda_t| = 0.040 \pm 0.003$, the branching ratio is

$$\mathcal{B}(B^0 \to \phi K_s^0) = (5.13 \pm 0.15) \times 10^{-3} \left| a_3 + a_4 + a_5 - \frac{1}{2}(a_7 + a_9 + a_{10}) - \frac{1}{2}(a'_7 + a'_9 + a'_{10}) \right|^2 . \tag{62}$$

The range of $\mathcal{S}_{\phi K}$ obtained for $N_{eff} = 2, 3, \ldots 10$ is shown in Figure 11, and is plotted against the branching ratio. CLEO, BABAR, and BELLE have recently measured this branching ratio[62, 63], and the average of their results is $\mathcal{B}(B^0 \to \phi K^0) = (8.7 \pm 1.3) \times 10^{-6}$.

We find that a range $0.2 \lesssim \mathcal{S}_{\phi K} \lesssim 1.0$ can be explained by FCNC's in this model while simultaneously accommodating semi-leptonic B decay and $B \to \phi K$ branching fraction data at the 2-σ level. While the shift in $\mathcal{S}_{\phi K}$ from FCNC's is not large enough to completely explain the current experimental value, it is still significant, and reduces the discrepancy to below 2-σ. A strong phase, δ, in the new physics relative to the SM would only decrease the range of

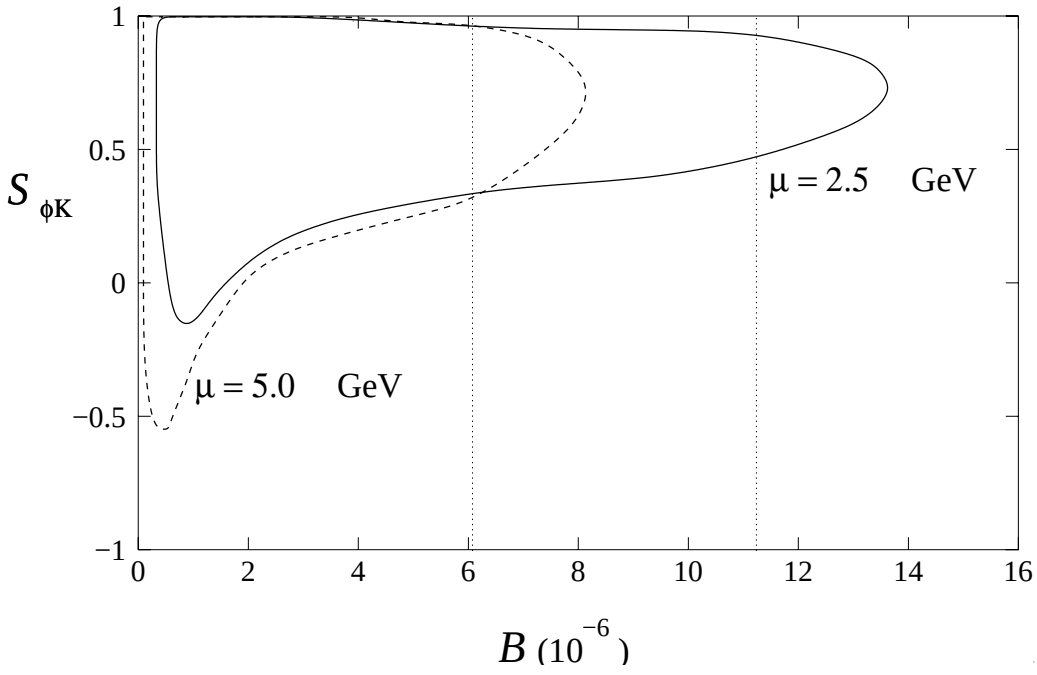

Figure 11: Range of $\mathcal{S}_{\phi K}$ accessible by the model plotted against the branching ratio for two choices of the renormalization scale. The vertical dotted lines indicate the 2-σ allowed region for the branching ratio.

$\mathcal{S}_{\phi K}$ [63]. Setting $\delta = \pi$ gives a result similar to that displayed in Fig. 11. The result shows a strong dependence on the renormalization scale, μ, as well as the effective number colours, N_{eff} due to sensitive cancellations between terms in the amplitude. While this situation would be improved by adding higher order corrections, we do not expect such terms to change these general conclusions.

The above result is more constraining than the one obtained in Ref. [64], in which the effect of a vector-like pair of singlet down quarks on $\mathcal{S}_{\phi K}$ was considered. As we have done here, these authors investigate the range of $\mathcal{S}_{\phi K}$ that can be obtained from the sZb vertex that is induced by vector-like down quarks. Our results should reduce to theirs in the limit $\eta' \to 0$, which corresponds to considering only the flavour mixing effects due to the singlets. By the same reasoning, the range of $\mathcal{S}_{\phi K}$ should be greater in the present model since even more flavour mixing is possible. Instead, these authors find a larger range for $\mathcal{S}_{\phi K}$ than we have obtained. One of the possible sources of discrepancy between our analysis and the one in Ref. [64] resides in our use of a more stringent quantitative analysis of the constraints

coming from the semileptonic B-decays. Another source appears to be their inclusion of the "colour-suppressed" operators $(\bar{s}_\beta b_\alpha)_{(V-A)}(\bar{s}_\alpha s_\beta)_{(V\pm A)}$ at tree-level. While such operators do arise from QCD corrections to the sZb vertex, all tree-level effects may be described by the "colour allowed" operators $(\bar{s}_\beta b_\beta)_{(V-A)}(\bar{s}_\alpha s_\alpha)_{(V\pm A)}$.

7 Conclusion

We have investigated the phenomenological properties of Beautiful mirrors, an extension of the Standard Model consisting of additional vector-like "mirror" quarks with the same quantum numbers as the $SU(2)$ quark doublet and down quark singlet in the Standard Model. These exotic quarks mix with the bottom quark resulting in a modified value of the right-handed bottom quark coupling to the Z gauge boson, in agreement with indications coming from the precision electroweak data. A good fit to the precision electroweak data also demands that the additional quarks have masses lower than about 300 GeV implying a rich phenomenology at the Tevatron and LHC Colliders, as well as a possible impact on the CP-violating observables measured at the B-factories. In addition, the unification of gauge couplings is greatly improved within the model.

In this article we have provided a detailed analysis of the question of gauge coupling unification. We find that the gauge couplings unify at $M_G = (2.80 \pm 0.15) \times 10^{16}$ GeV. Perturbative consistency and stability of the model restrict the possible values of the masses of the Higgs and the mirror quarks. The allowed range, $m_h = 170 \pm 10$ GeV, overlaps with the range of values of these parameters which give the best fit to precision electroweak data [6].

Flavour mixing due to the mirror quarks leads to right-handed Z couplings, a very small loss of unitarity of the CKM matrix, and FCNCs. The flavour mixing also modifies the coupling of the b and ω quarks to the Higgs, while the couplings of the other quarks to the Higgs are not changed significantly. This has some interesting implications for Higgs searches at the Tevatron. In particular, the required luminosity for a Tevatron or LHC Higgs discovery in the WW decay mode, as well as in the $\tau^+\tau^-$ mode at the Tevatron and the $\gamma\gamma$ mode at the LHC, is greatly reduced within this model. We have analyzed the search for mirror vector quarks at the Tevatron collider, and have found that Run II with a total integrated luminosity of about 4 fb^{-1} will be able to test all of the mirror quark mass range consistent with electroweak precision data. Finally, the $b \to s$ FCNCs which arise in this model can help explain the discrepancy between the values of $\sin(2\beta)$ measured in the $B \to \phi K$ and $B \to J/\psi K$ decays.

Acknowledgements The authors would like to thank M. Carena, Z. Chacko, C.W. Chiang, D. Choudhury, D.E. Kaplan. T. Le Compte, R. Sundrum and T.M.P. Tait for interesting comments and suggestions. Work supported in part by the US DOE, Div. of HEP, Contract W-31-109-ENG-38.

Note added : As this work was being completed, Ref. [65] appeared, in which the effect of tree-level ($V \pm A$) sZb couplings on $\mathcal{S}_{\phi K}$ was calculated. The modifications to the electroweak scale Wilson coefficients as well as the final result in this paper agree with our analysis.

References

[1] LEP Electroweak Working Group, LEPEWWG/2003-01.

[2] H. E. Haber and H. E. Logan, Phys. Rev. D **62**, 015011 (2000) [hep-ph/9909335].

[3] M. S. Chanowitz, Phys. Rev. Lett. **87**, 231802 (2001) [arXiv:hep-ph/0104024].

[4] G. Altarelli, F. Caravaglios, G. F. Giudice, P. Gambino and G. Ridolfi, JHEP **0106**, 018 (2001) [arXiv:hep-ph/0106029].

[5] M. Carena, E. Ponton, T. M. Tait and C. E. M. Wagner, arXiv:hep-ph/0212307.

[6] D. Choudhury, T. M. Tait and C. E. Wagner, Phys. Rev. D **65**, 053002 (2002) [arXiv:hep-ph/0109097].

[7] L. Randall and R. Sundrum, Phys. Rev. Lett. **83**, 3370 (1999) [arXiv:hep-ph/9905221].

[8] A. Pomarol, Phys. Rev. Lett. **85**, 4004 (2000) [arXiv:hep-ph/0005293]. L. Randall and M. D. Schwartz, JHEP **0111**, 003 (2001) [arXiv:hep-th/0108114]; Phys. Rev. Lett. **88**, 081801 (2002) [arXiv:hep-th/0108115]; K. w. Choi, H. D. Kim and Y. W. Kim, JHEP **0211**, 033 (2002) [arXiv:hep-ph/0202257]; arXiv:hep-ph/0207013; K. Agashe, A. Delgado and R. Sundrum, Nucl. Phys. B **643**, 172 (2002) [arXiv:hep-ph/0206099]; R. Contino, P. Creminelli and E. Trincherini, JHEP **0210**, 029 (2002) [arXiv:hep-th/0208002]; A. Falkowski and H. D. Kim, JHEP **0208**, 052 (2002) [arXiv:hep-ph/0208058]; K. w. Choi and I. W. Kim, Phys. Rev. D **67**, 045005 (2003) [arXiv:hep-th/0208071]; L. Randall, Y. Shadmi and N. Weiner, JHEP **0301**, 055 (2003) [arXiv:hep-th/0208120];

A. Lewandowski, M. J. May and R. Sundrum, Phys. Rev. D **67**, 024036 (2003) [arXiv:hep-th/0209050]; K. Agashe and A. Delgado, Phys. Rev. D **67**, 046003 (2003) [arXiv:hep-th/0209212].

[9] W. D. Goldberger and I. Z. Rothstein, Phys. Rev. Lett. **89**, 131601 (2002) [arXiv:hep-th/0204160]; arXiv:hep-th/0208060; arXiv:hep-ph/0303158.

[10] K. Agashe, A. Delgado and R. Sundrum, Annals Phys. **304**, 145 (2003) [arXiv:hep-ph/0212028].

[11] M. Carena, A. Delgado, E. Ponton, T. M. Tait and C. E. Wagner, arXiv:hep-ph/0305188.

[12] H. Arason, D. J. Castano, B. Keszthelyi, S. Mikaelian, E. J. Piard, P. Ramond and B. D. Wright, Phys. Rev. D **46**, 3945 (1992).

[13] M. E. Machacek and M. T. Vaughn, Nucl. Phys. B **222**, 83 (1983).

[14] M. E. Machacek and M. T. Vaughn, Nucl. Phys. B **236**, 221 (1984).

[15] M. E. Machacek and M. T. Vaughn, Nucl. Phys. B **249**, 70 (1985).

[16] G. Cvetic, C. S. Kim and S. S. Hwang, Phys. Rev. D **58**, 116003 (1998) [arXiv:hep-ph/9806282].

[17] K. Hagiwara *et al.* [Particle Data Group Collaboration], Phys. Rev. D **66**, 010001 (2002).

[18] L. J. Hall, Nucl. Phys. B **178**, 75 (1981);

P. Langacker and N. Polonsky, Phys. Rev. D **47**, 4028 (1993) [arXiv:hep-ph/9210235].

M. Carena, S. Pokorski and C. E. Wagner, Nucl. Phys. B **406**, 59 (1993) [arXiv:hep-ph/9303202].

[19] P. H. Frampton, P. Q. Hung and M. Sher, Phys. Rept. **330**, 263 (2000) [arXiv:hep-ph/9903387].

[20] Y. Suzuki *et al.* [TITAND Working Group Collaboration], arXiv:hep-ex/0110005.

[21] See, for example, P. Nath and R. Arnowitt, Phys. Rev. Lett. **70**, 3696 (1993) [arXiv:hep-ph/9302318]; R. Dermisek, A. Mafi and S. Raby, Phys. Rev. D **63**, 035001 (2001) [arXiv:hep-ph/0007213]; H. Murayama and A. Pierce, Phys. Rev. D **65**, 055009 (2002) [arXiv:hep-ph/0108104]; and references therein.

[22] S. Raby, arXiv:hep-ph/0211024.

[23] D. Emmanuel-Costa and S. Wiesenfeldt, arXiv:hep-ph/0302272; P. Langacker, Phys. Rept. **72**, 185 (1981).

[24] S. Aoki *et al.* [JLQCD Collaboration], Phys. Rev. D **62**, 014506 (2000) [arXiv:hep-lat/9911026].

[25] F. Wilczek and A. Zee, Phys. Rev. Lett. **43**, 1571 (1979).

[26] F. Larios, M. A. Perez and C. P. Yuan, Phys. Lett. B **457**, 334 (1999) [hep-ph/9903394].

[27] J.F. Gunion, H.E. Haber, G. Kane, S. Dawson, The Higgs Hunter's Guide, Perseus Books, 1990. J. F. Gunion, H. E. Haber, G. L. Kane and S. Dawson, SCIPP-89/13

[28] A. Djouadi, M. Spira and P. M. Zerwas, Phys. Lett. B **264**, 440 (1991).

[29] D. Rainwater, M. Spira and D. Zeppenfeld, arXiv:hep-ph/0203187;

[30] M. Carena and H. E. Haber, arXiv:hep-ph/0208209.

[31] A. Belyaev, T. Han and R. Rosenfeld, arXiv:hep-ph/0204210.

[32] M. Carena *et al.* [Higgs Working Group Collaboration], arXiv:hep-ph/0010338.

[33] M. Carena, J. R. Ellis, S. Mrenna, A. Pilaftsis and C. E. Wagner, arXiv:hep-ph/0211467.

[34] K.Jakobs, T. Trefzger, ATL-PHYS-2000-015

[35] T. Affolder *et al.* [CDF Collaboration], Phys. Rev. Lett. **84**, 835 (2000) [arXiv:hep-ex/9909027].

CDF Collaboration, T.Affolder *et al.*, Phys. Rev. Lett. **84**, 835 (2000) [hep-ex/9909027].

[36] E. L. Berger and H. Contopanagos, Phys. Rev. D **57**, 253 (1998) [arXiv:hep-ph/9706206].

[37] N. Kidonakis, in *Proc. of the APS/DPF/DPB Summer Study on the Future of Particle Physics (Snowmass 2001)* ed. N. Graf, eConf **C010630**, P505 (2001) [arXiv:hep-ph/0110145].

[38] K. Sliwa [CDF Collaboration], Acta Phys. Polon. B **33**, 3861 (2002).

[39] P. Savard [CDF and D0 collaborations], eConf **C020620**, SABT05 (2002) [arXiv:hep-ex/0209061].

[40] T. Affolder *et al.* [CDF Collaboration], Phys. Rev. Lett. **84**, 216 (2000) [arXiv:hep-ex/9909042].

[41] G. L. Kane, G. A. Ladinsky and C. P. Yuan, Phys. Rev. D **45**, 124 (1992).

[42] M. Sher, Phys. Rev. D **61**, 057303 (2000) [arXiv:hep-ph/9908238]; M. Sher, Phys. Rev. **D**61, 057303 (2000) [hep-ph/9908238].

[43] I. I. Bigi, Y. L. Dokshitzer, V. A. Khoze, J. H. Kuhn and P. M. Zerwas, Phys. Lett. B **181**, 157 (1986).

[44] G. Hiller, Phys. Rev. D **66**, 071502 (2002) [arXiv:hep-ph/0207356].

[45] K. Abe *et al.* [Belle Collaboration], arXiv:hep-ex/0207098.

[46] B. Aubert *et al.* [BABAR Collaboration], arXiv:hep-ex/0207070.

[47] R. Fleischer, Phys. Rept. **370**, 537 (2002) [arXiv:hep-ph/0207108].

R. Fleischer and T. Mannel, Phys. Lett. B **511**, 240 (2001) [arXiv:hep-ph/0103121].

[48] G. Barenboim, F. J. Botella and O. Vives, Phys. Rev. D **64**, 015007 (2001) [arXiv:hep-ph/0012197];

J. A. Aguilar-Saavedra, Phys. Rev. D **67**, 035003 (2003) [arXiv:hep-ph/0210112].

[49] A. J. Buras and R. Fleischer, Adv. Ser. Direct. High Energy Phys. **15**, 65 (1998) [arXiv:hep-ph/9704376].

[50] T. Yanir, JHEP **0206**, 044 (2002) [arXiv:hep-ph/0205073].

[51] G. Buchalla, G. Hiller and G. Isidori, Phys. Rev. D **63**, 014015 (2001) [arXiv:hep-ph/0006136].

[52] A. Ali, P. Ball, L. T. Handoko and G. Hiller, Phys. Rev. D **61**, 074024 (2000) [arXiv:hep-ph/9910221].

[53] J. Kaneko *et al.* [Belle Collaboration], Phys. Rev. Lett. **90**, 021801 (2003) [arXiv:hep-ex/0208029].

[54] A. Ali, E. Lunghi, C. Greub and G. Hiller, Phys. Rev. D **66**, 034002 (2002) [arXiv:hep-ph/0112300].

[55] K. Abe *et al.* [BELLE Collaboration], Phys. Rev. Lett. **88**, 021801 (2002) [arXiv:hep-ex/0109026].

[56] B. Aubert *et al.* [BABAR Collaboration], arXiv:hep-ex/0207082.

[57] A. J. Buras, arXiv:hep-ph/9806471.

[58] A. J. Buras, M. Jamin and M. E. Lautenbacher, Nucl. Phys. B **400**, 75 (1993) [arXiv:hep-ph/9211321].

[59] M. Beneke, G. Buchalla, M. Neubert and C. T. Sachrajda, Nucl. Phys. B **606**, 245 (2001) [arXiv:hep-ph/0104110].

[60] A. Ali, G. Kramer and C. D. Lu, Phys. Rev. D **58**, 094009 (1998) [arXiv:hep-ph/9804363].

[61] H. Y. Cheng and K. C. Yang, Phys. Rev. D **64**, 074004 (2001) [arXiv:hep-ph/0012152].

[62] R. A. Briere *et al.* [CLEO Collaboration], Phys. Rev. Lett. **86**, 3718 (2001) [arXiv:hep-ex/0101032];

B. Aubert *et al.* [BABAR Collaboration], arXiv:hep-ex/0303029.

[63] C. W. Chiang and J. L. Rosner, arXiv:hep-ph/0302094.

[64] A. K. Giri and R. Mohanta, arXiv:hep-ph/0306041.

[65] D. Atwood and G. Hiller, arXiv:hep-ph/0307251.